Available online at www.sciencedirect.com
ScienceDirect
Mendeleev Commun., 2013, **23**, 334–336
Mendeleev Communications

Redox properties and radical anions of 2-substituted thioxanthen-9-ones and their 2-methyl *S*-oxide derivatives

Nadezhda V. Vasilieva, Irina G. Irtegova, Vladimir A. Loskutov and Leonid A. Shundrin*

N. N. Vorozhtsov Institute of Organic Chemistry, Siberian Branch of the Russian Academy of Sciences, 630090 Novosibirsk, Russian Federation. Fax: +7 383 330 9752; e-mail: shundrin@nioch.nsc.ru

DOI: 10.1016/j.mencom.2013.11.010

The electrochemical reduction of 2-substituted thioxanthen-9-ones in MeCN is a one-electron process with the formation of long-lived radical anions, in which the thioxanthen-9-one fragment is planar according to EPR measurements and UB3LYP/6-31+G* calculations. The electrochemical reduction of 2-methylthioxanthen-9-one sulfoxide and sulfone are EEC and EE processes, respectively, their radical anions are not planar, and the electrochemical oxidation of the title compounds is irreversible with consecutive oxidation of the sulfur atom, except for the sulfone, whose oxidation was not observed at the limit of the anodic potential (2.5 V *vs.* s.c.e.).

The derivatives of thioxanthen-9-ones (thioxanthones) are used as efficient photoinitiators for free radical polymerization[1] and as photogenerators for detrilation in oligonucleotide microarray synthesis.[2,3] Thioxanthone derivatives possess a biological activity inhibiting the multidrug efflux pump activity in *Staphylococcus*,[4] and they are used for the treatment of infectious diseases.[5] On the other hand, thioxanthones and their *S*-oxides can be reduced by a one-electron transfer mechanism to form long-lived radical anions (RAs),[6,7] *i.e.*, these compounds can be considered as substances with the active electron transport function in living organisms. The potentials of electrochemical reduction (ECR) and electrochemical oxidation (ECO) of thioxantone and related compounds in MeCN and other solvents have been described,[8–10] and a good correspondence between experimental potentials and LUMO/HOMO energies of thioxanthones calculated by semi-empirical,[9] *ab initio* Hartree–Fock and DFT methods[12,13] has been demonstrated. The EPR spectra of the RAs of unsubstituted thioxanthone and corresponding sulfoxide and sulfone have been obtained.[6,7] Nevertheless, the RAs of substituted thioxanthone and its *S*-oxides have not been described correctly, and the mechanisms of ECR and ECO of thioxanthone sulfoxide and its derivatives in aprotic solvents have not been studied. In the proposed earlier scheme of two-electron ECO of thioxanthone the first oxidative peak only for potential scan limit up +2.0 V was described,[9] whereas the subsequent steps of ECO at more positive potentials were not considered. To make up this deficiency we studied redox properties and RAs of 2-substituted thioxanthones, 2-methylthioxanthone sulfoxide and 2-methylthioxanthone sulfone in MeCN[†] by cyclic voltammetry and EPR spectroscopy.

The ECR[‡] of **1a–d** is characterized by one electron reversible [Figure 1(*a*), **1d**] or quasi-reversible peak [$E_p^{1A} - E_p^{1C} = 0.06$ V,

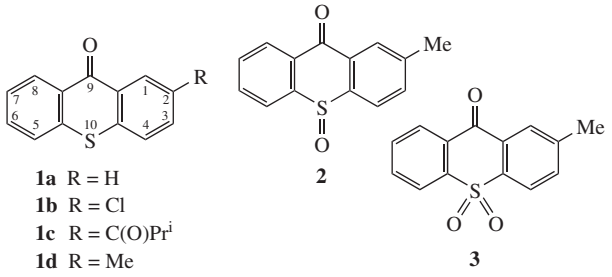

1a R = H
1b R = Cl
1c R = C(O)Pr^i
1d R = Me

2

3

$I_p^{1A}/I_p^{1C} \approx 0.8–0.9$ (**1a–c**), $\nu = 0.1$ V s^{-1}][§] within the potential sweep range $0 > E > -2.0$ V. Corresponding peak potentials are listed in Table S1 (see Online Supplementary Materials). Cyclic voltammogram (CV) of **2** is characterized by two reduction peaks (1C, 2C) in the same potential sweep range [Figure 1(*b*)], the peak current ratio $I_p^{1A}/I_p^{1C} = 0.23$ at $\nu = 0.1$ V s^{-1} within the above potential sweep. CV wave 1C–1A becomes completely reversible ($E_p^{1A}–E_p^{1C} = 0.06$ V, $I_p^{1A}/I_p^{1C} = 1.0$), if the potential sweep range does not reach E_p^{2C} ($0.0 > E > -1.6$ V) [Figure 1(*b*)]. The first one-electron peak (1C) corresponds to the formation of RA **2** in accordance with EPR data[¶] [Figure 2(*b*)]. CVs of **2** measured at different potential scan rates[§] demonstrated that peak 2C corresponds to the formation of dianion (DA) **2** with the subsequent protonation and the formation of **1d** as a result. The latter was proved by CV of **2** in the range of potential sweep involving both reduction and oxidation processes because a minor irreversible oxidative peak [1A′(Ox), $E_p^{1A'(Ox)} = 1.62$ V] corresponding to the ECO of **1d** was observed in the anodic branch of CV. This peak was not observed if the potential sweep did not cover second reduction peak 2C [Figure 1(*c*)]. The EPR measurements[¶] of paramagnetic species obtained under ECR of **2** at the potential of

[†] Compounds **1a**,**c**,**d**, **2**, **3** were prepared as described elsewhere,[13,14] commercial **1b** from Aldrich was used.

[‡] The CV measurements of **1–3** (2.0 mM solutions) were performed at 298 K in an argon atmosphere in MeCN purified by a standard procedure (MeCN was distilled from $KMnO_4$ and twice from P_2O_5, the residual water content was 5 mM) at a stationary Pt disk electrode ($S = 0.08$ cm^2) with 0.1 M Et_4NClO_4 as a supporting electrolyte with potential sweep rates of $0.1 < \nu < 1.2$ V s^{-1}. A PG 310 USB potentiostat (HEKA Elektronik GmbH, Germany) was used for CV measurements. A standard electrochemical cell (solution volume of 5 ml) connected to the potentiostat with a three-electrode scheme was used. Peak potentials are quoted with reference to a saturated calomel electrode (s.c.e). iR compensation has not been taken into account for the peak potentials presented in Table S1. Reduction peaks are diffusion controlled for **1–3**, *i.e.*, $I_p^{1C}\nu^{-0.5}$ = const, where I_p^{1C} is the peak current. Digital simulation of the CV of **1d** in oxidative potentials area was done using electrochemical simulation Package (ESP, v.2.4) designed by Carlo Nervi, Università di Torino, Italy. Simplex algorithm was used for multiparametric optimization implemented in the package. Digital simulation of the CV of **1d** [Figure 1(*b*)] is shifted for –50 μA for better clearness.

[§] For CV of **1a–c**, CV of **2** at various ν, the EPR spectra of RAs **1a–c**, digital simulation details for CV of **1d** in oxidative potentials area, discussion about disproportionation mechanism of the ECO of **2**, see Online Supplementary Materials.

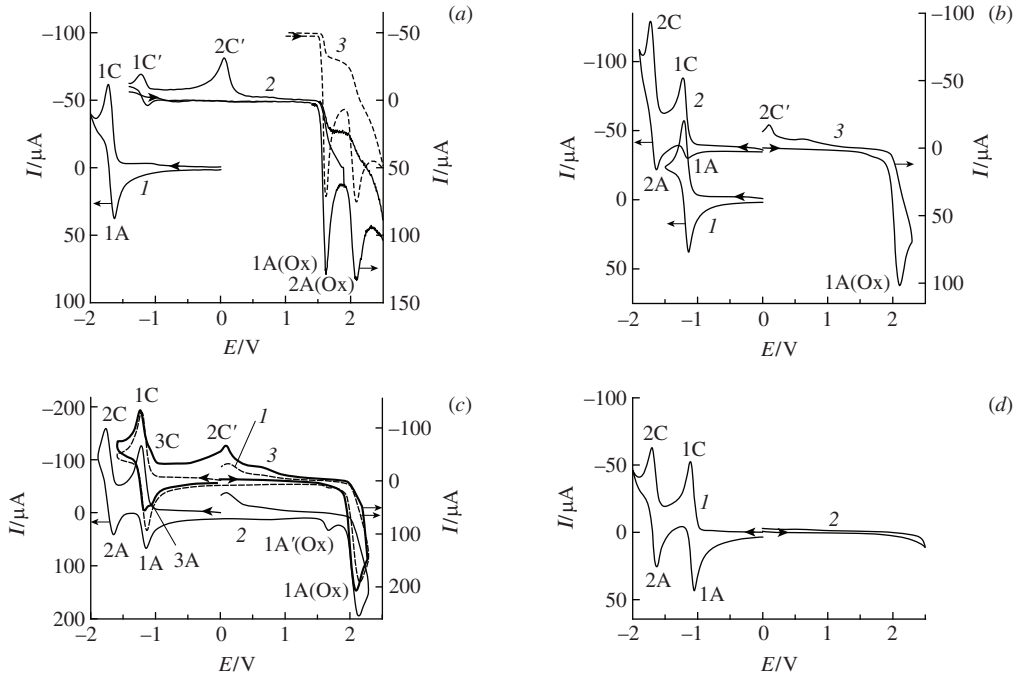

Figure 1 (*a*) CV of **1d** (2.0 mM) in MeCN (v = 0.1 V s^{-1}) within potential sweep regions (*1*) 0.0 > *E* > –2.0 V, (*2*) –1.4 < *E* < 2.5 V and (*3*) digital simulation of the CV of **1d** in oxidative potentials area. (*b*) CV of **2** in MeCN (v = 0.1 V s^{-1}) within potential sweep regions (*1*) 0.0 > *E* > –1.6 V, (*2*) 0.0 > *E* > –1.9 V and (*3*) 0.0 < *E* < 2.3 V. (*c*) CV of **2** (v = 0.5 V s^{-1}) within wide potential sweep cycle *E*: (*1*) 0.0 → –1.6 → 2.3 → 0.0 V, (*2*) 0.0 → –1.9 → 2.3 → 0.0 V, and (*3*) 0.0 → 2.3 → –1.6 → 0.0 V. (*d*) CV of **3** in MeCN (v = 0.1 V s^{-1}) within potential sweep regions (*1*) 0.0 > *E* > –2.0 V and (*2*) 0.0 < *E* < 2.5 V.

2C peak verified the formation of **1d** at the second step of ECR because a mixed EPR spectrum from RAs **2** and **1d** (10 and 90% of the total ERP signal intensity, respectively) was observed [Figure 2(*c*)]. The total current of peak 2C includes the dominating contribution from ECR of **2** to DA **2** and a minor contribution from one-electron ECR of **1d** because the latter process is characterized by a potential close to the potential of peak 2C [Figure 1(*a*),(*b*), Table S1]. As a result, peak current ratio I_p^{2C}/I_p^{1C} = 1.38 at v = 0.1 V s^{-1} [Figure 1(*b*)] and tends to 1 when v is increased.§ The ECR of **3** is an EE process with two well separated one-electron and diffusion-controlled peaks corresponding to the formation of RA and DA of **3**, respectively [Figure 1(*d*)].

The RAs of **1**–**3** were obtained by the one-electron ECR of neutral precursors in MeCN (Figure 2).§ The corresponding hyperfine coupling constants (HFCC) with ^{1}H nuclei are in a good agreement with those calculated by the UB3LYP/6-31+G* method (Table S2, see Online Supplementary Materials).¶ In accordance with the calculations, the thioxanthone fragment is planar in optimized conformations of RAs **1a**–**d** [Figure 3(*a*)] and their single occupied molecular orbital (SOMO) is of the π-type. The presence of oxygen atoms in the 10-position of RAs **2** and **3** leads to a bending of their structure along the axis O–C(9)–S and pyramidal structure of sulfoxide and sulfone fragments. The dihedral angles between aromatic rings are 10.2° and 16.6° in RAs **2** and **3**, respectively [Figure 3(*b*),(*c*)], and SOMO is of the pseudo π-type. Calculated spin density distribution is dominated by the C=O group with a smaller contribution from carbon atoms in the 1-, 3-, 6- and 8-positions of RAs **1d**, **2**, **3** (Figure 3). The largest HFCCs are related to the protons in the above positions for all of the test RAs, and the presence of SO and SO_2 groups in RA **2**, **3** leads to a decrease in HFCC with ^{1}H nuclei in these positions (Table S2).

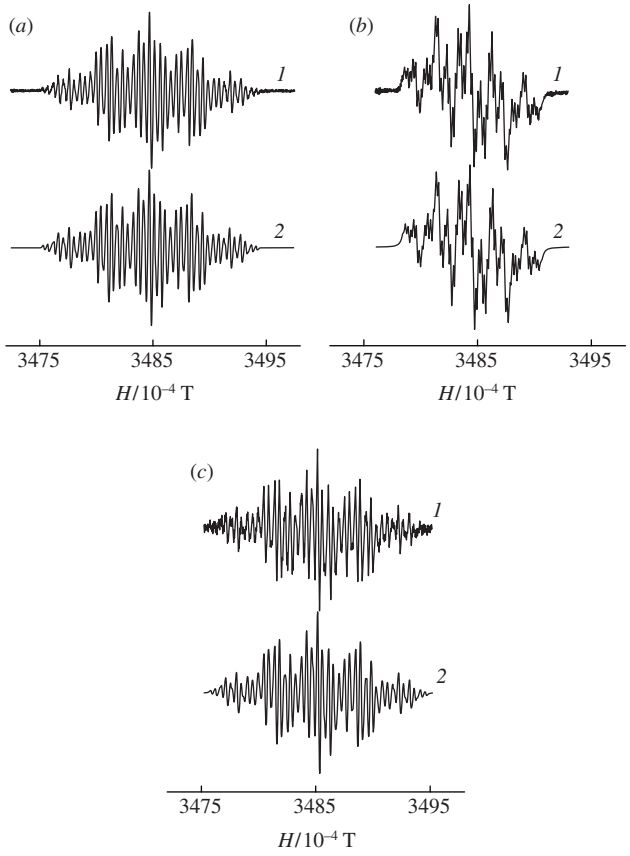

Figure 2 EPR spectra of RAs (*a*) **1d**, (*b*) **2** and (*c*) a mixed spectrum of RAs **1d**, **2** (90 and 10% of intensity, respectively) obtained under ECR at the potential of 2C peak: (*1*) experimental and (*2*) simulated spectrum.

¶ The EPR spectra were recorded on a Bruker ELEXSYS E-540 X-band spectrometer (MW power of 20 mW, modulation frequency of 100 KHz and modulation amplitude of 0.005 mT). RAs of **1**–**3** were obtained by ECR in MeCN under argon atmosphere at 298 K with the standard electrochemical cell for EPR measurements. Simulations of the experimental EPR spectra were performed with the Winsim 2002 program[15] (the accuracy in calculating of HFCC is ±0.0001 mT). The quantum-chemical calculations were performed using the GAMESS suite of programs.[16] The geometries of RAs **1**–**3** were fully optimized at the UB3LYP/6-31+G* level of theory for gas phase. The symbols «+» and «–» (Figure 3) indicate the signs of spin density. Lowding charges at carbon, oxygen and sulfur atoms in RAs **1**–**3** are presented in Online Supplementary Materials (Table S3).

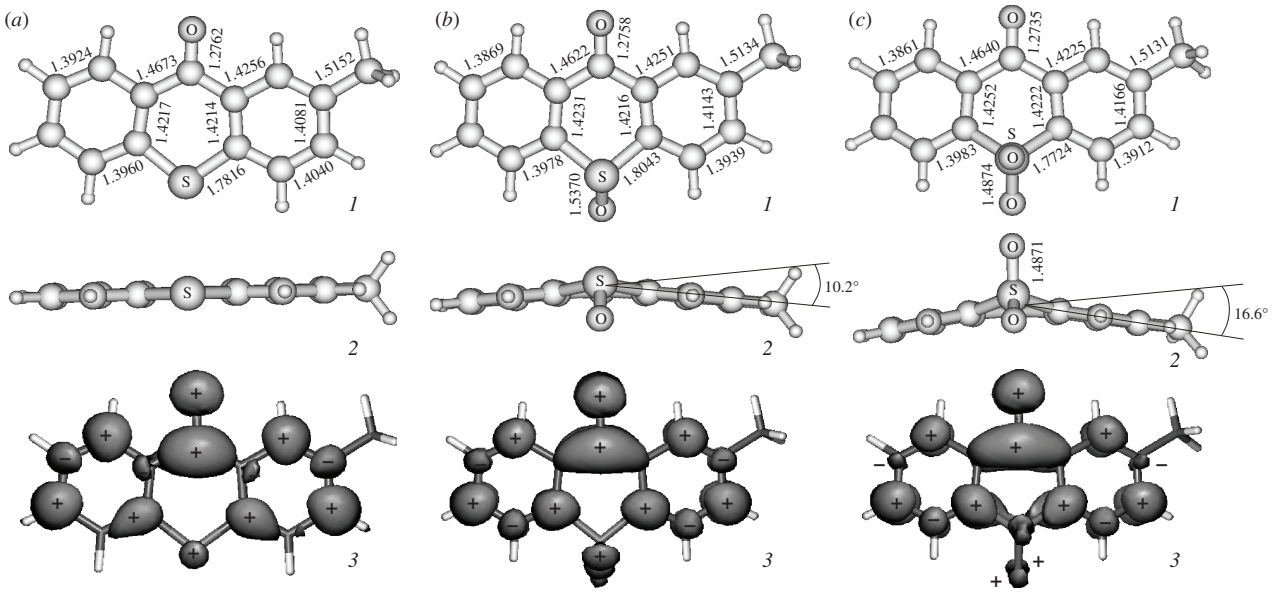

Figure 3 (*1*) UB3LYP/6-31+G* geometry, (*2*) view along O–C(9)–S axis and (*3*) distribution of spin density in RAs (*a*) **1d**, (*b*) **2** and (*c*) **3**. The bond lengths are given in Å.

The ECO of **1a–d** is characterized by two or, in some cases, three[§] (Table S1) irreversible peaks [Figure 1(*a*)] within the potential sweep range $0 < E < 2.5$ V. Digital simulation of the CV of **1d** in the potential sweep range $1.0 < E < 2.5$ V [Figure 1(*a*)] demonstrated that the first irreversible peak is two-electron, and it corresponds to the formation of **2**. As the proof of it, the change in potential sweep range up to $-1.4 < E < 1.8$ V results in the appearance of a one-electron reversible peak (1C′) in CV of **1d**, which conforms to the ECR of **2** [Figure 1(*a*)]. The second oxidative peak of **1d** is noticeably wider than the first one. According to a simulation, the 2A(Ox) peak in CV of **1d**, being two-electron as a whole, includes two one-electron irreversible peaks with close potentials corresponding to the consecutive ECO of **2** up to **3**. For this reason, two irreversible oxidative peaks are observed in the second step of the ECO for compounds **1a**,**b**,[§] for which the total process of ECO is three-step and four-electron. CV of **2** ($0.0 < E < 2.5$ V) reveals the only irreversible two-electron oxidative peak [Figure 1(*b*)], the potential of which is the same as the potential of 2A(Ox) peak in the CV of **1d** (Table S1). The expansion of potential sweep to the range covering the oxidation and first reduction steps of **2** ($-1.6 < E < 2.3$ V) leads to the superimposed reversible reduction CV waves corresponding to the one-electron reduction of **3** (3C–3A) and **2** (1C–1A) [Figure 1(*c*), curve *3*]. Thus, the second ECO stage of **1d** and the first stage of **2** correspond to the formation of **3** in agreement with the proposed earlier common scheme of multielectron ECO for unsubstituted thioxanthene.[9] Note that the ECO of **2** can proceed by a disproportionation mechanism, which is not preferable from the kinetic point of view.[§] No peaks were observed in the CV of **3** within the potential sweep range $0 < E < 2.5$ V [Figure 1(*d*)]. The nature of the reductive peak (2C′), which was detected at the cathodic branch of CV of **1a–d**,[§] **2** [Figure 1(*a*),(*b*)] is not clear. This peak was observed but not interpreted earlier in the CV of unsubstituted thioxanthone.[8] Note that the replacement of a supporting electrolyte by Bu_4NBF_4 resulted in the absence of 2C′ peak from the CV of **1d**.

Thus, the ECR of thioxanthones **1a–d** is characterized by reversible or quasi-reversible one-electron transfer in the potential sweep range $0 > E > -2.0$ V, whereas the ECR of **2**, **3** is a EEC- or EE-process, respectively. RAs **1a–d** have the planar structure of the thioxanthone fragment, but RAs **2**, **3** are not planar with SOMO of the pseudo-π type. The ECO of **1a–d** is two or three stage four-electron irreversible process with the formation of corresponding thioxanthone sulfoxides and sulfones in the potential sweep range $0 < E < 2.5$ V, sulfoxide **2** is oxidized to **3**, and **3** is not oxidized in the above potential sweep range.

Online Supplementary Materials

Supplementary data associated with this article can be found in the online version at doi:10.1016/j.mencom.2013.11.010.

References

1 Q. A. Sun, J. T. Wang, L. M. Zhang and M. P. Yang, *Acta Phys. Chim. Sin*., 2010, **26**, 2481.
2 A. N. Sinyakov, A. A. Ryabinin, G. A. Maksakova, V. V. Shelkovnikov, V. A. Loskutov, E. V. Vasil'ev and N. V. Shekleina, *Russ. J. Bioorg. Chem*., 2010, **36**, 130 (*Zh. Bioorg. Khim*., 2010, **36**, 139).
3 V. V. Shelkovnikov, V. A. Loskutov, E. V. Vasil'ev, N. V. Shekleina, V. A. Ryabinin and A. N. Sinyakov, *Russ. Chem. Bull., Int. Ed*., 2011, **60**, 561 (*Izv. Akad Nauk, Ser. Khim.*, 2011, 548).
4 G. W. Kaatz, V. V. Moudgal, S. M. Seo and J. E. Kristiansen, *Antimicrob. Agents Chemother*., 2003, **47**, 719.
5 B. K. Giwercman, *US Patent 2012/0122880 A1*, 2010 (*Chem. Abstr.*, 2010, **153**, 554920).
6 M. M. Urberg and E. T. Kaiser, *J. Am. Chem. Soc.*, 1967, **89**, 5179.
7 T. Aruga, O. Ito and M. Matsuda, *J. Am. Chem. Soc.*, 1979, **101**, 7585.
8 P. T. Kissinger, P. T. Holt and C. N. Reilley, *J. Electroanal. Chem*., 1971, **33**, 1.
9 E. W. Tsai, L. Throckmorton, R. McKellar, M. Baar, M. Kluba, D. S. Marynick, K. Rajeshwar and A. L. Ternay, Jr., *J. Electroanal. Chem.*, 1986, **210**, 45.
10 N. V. Vasilieva, I. G. Irtegova, V. A. Loskutov and L. A. Shundrin, *Mendeleev Commun*., 2012, **22**, 111.
11 K.-D. Kwak, M. L. Seo, K. S. Ha and U.-H. Paek, *Bull. Korean Chem. Soc.*, 1998, **19**, 527.
12 S. Riahi, P. Norouzi, A.B. Moghaddam, M.R. Ganjali, G.R. Karimipour and H. Shargi, *Chem. Phys.*, 2007, **337**, 33.
13 R. Ran and Ch. U. Pittman, Jr., *J. Heterocycl. Chem*., 1993, **30**, 1673.
14 (*a*) V. A. Loskutov and V. V. Shelkovnikov, *Russ. J. Org. Chem.*, 2006, **42**, 298 (*Zh. Org. Khim.*, 2006, **42**, 313); (*b*) V. A. Loskutov and V. V. Shelkovnikov, *Russ. J. Org. Chem*., 2009, **45**, 158 (*Zh. Org. Khim*., 2009, **45**, 160).
15 D. R. Duling, *J. Magn. Reson*., 1994, **104**, 105.
16 M. W. Schmidt, K. K. Baldridge, J. A. Boatz, S. T. Elbert, M. S. Gordon, J. H. Jensen, S. Koseki, N. Matsunaga, K. A. Nguyen, S. J. Su, T .L. Windus, M. Dupuis and J. A. Montgomery, *J. Comput. Chem.*, 1993, **14**, 1347.

Received: 6th May 2013; Com. 13/4116